

Received October 1, 2020, accepted October 13, 2020, date of publication October 27, 2020, date of current version November 10, 2020.

Digital Object Identifier 10.1109/ACCESS.2020.3034228

# Relative Pose Estimation Based on Pairwise Range With Application to Aerobridge

**RUCAN XIA AND HAILONG PEI, (Member, IEEE)**

Key Laboratory of Autonomous Systems and Network Control, Ministry of Education, South China University of Technology, Guangzhou 510640, China  
Unmanned System Engineering Center of Guangdong Province, South China University of Technology, Guangzhou 510640, China  
School of Automation, South China University of Technology, Guangzhou 510640, China

Corresponding author: Hailong Pei (auhpei@scut.edu.cn)

This work was supported in part by the Scientific Instruments Development Program of NSFC under Grant 615278010, and in part by the Science and Technology Planning Project of Guangdong, China, under Grant 2017B010116005.

**ABSTRACT** Relative pose estimation refers to estimate the relative attitude and translation between multiple platforms. For mobile platforms, tracking the relative pose with pairwise range is challenging for highly nonlinear associations between measurement and state. This article proposes a promising framework using pairwise range to estimate the relative pose parameterized with Lie algebra. It is compatible with the existing Gauss-Newton method and the Levenberg–Marquardt method. We analyze the existence of the optimal solution based on the rank of the Hessian matrix, which turns into a discussion of sensors placement. The associated unconstrained Cramer-Rao Lower Bound with fewer variables is presented. To track moving platforms, we derived a novel and accurate relative kinematics without angular accelerations. An extended Kalman filter incorporating the measurement of an IMU is designed to generate smooth poses. A simplified version of the optimizer with less dimension is introduced to the application of aerobridge, which is also compatible with other multilink devices. Simulations verify the proposed algorithm and the comparisons with the existing popular methods prove its novelty.

**INDEX TERMS** Cramer-Rao lower bound, extended Kalman filter, nonlinear optimization, relative pose estimation, wireless sensors network.

## I. INTRODUCTION


Pose estimation (rigid body localization), i.e. guessing the attitude and translation, is a well-studied subject in the robotic field and Astronautics community for several decades. It is widely applied in military, industry, and civilian applications, such as guided missiles, unmanned aerial vehicles, floor mopping robot, etc. It has been challenging since the pose associates with measurements nonlinearly in general and follows some quadratic constraint [1].

Absolute and relative pose estimation are two branches and they differ in whether the reference frame is moving. Absolute pose estimation is conventionally solved with a set of GPS, accelerometers, and magnetometers, which can work in a long-distance circumstance but rarely perform indoor for the degeneration of GPS and the magnetic-field interference. Relative pose estimation usually occurs in a short-distance circumstance (indoor and outdoor) where camera and wireless sensors network (WSN) are capable. Since every frame

move, the inertial measurement unit (IMU) is used to capture the high dynamic character.

The traditional approaches separately estimate attitudes and positions [3], [4]. Most closed-form solutions of attitude consider solving the least-square problem, named Wahba's problem [5], to minimize the deviation of the line-of-sights measurements and its prediction. Typical methods including closed-form quaternion [6], TRIAD algorithm [7], q-method [8], etc. Then the optimal translation is the displacement between the centroid of the coordinates in one frame and the rotated and scaled centroid of the coordinates in the other frame [6]. Recently, advanced WSN prompts high accuracy localization. For example, the WSN with ultrawideband (UWB) sensors can generate centimeter-level measurement and therefore produce a precise pose estimation [9].

Most rigid bodies are not standstills [1] in practice, so pose tracking attracts considerable attention. Chepuri *et al.* proposed Kalman filters (KFs) incorporating the range measurements, angular and translational velocity to estimate the pose. The unitary constraint causes the attitude and translation to be estimated separately and measuring the translational velocity

The associate editor coordinating the review of this manuscript and approving it for publication was Razi Iqbal .

directly is impractical in general [4]. Chen and Ho present a divide and conquer (DAC) method to estimate the pose, angular velocity, and translational velocity using Doppler measurements [1]. In [2], they developed a specialized DAC with less complexity but the performance is not better than [1]. Recently, Jiang *et al.* propose a robust semidefinite relaxation (SDR) to harsh localization scenarios over a large range of noise levels [15]. Furthermore, the convex semidefinite program (SDP) is formulated and the SDR method is used to obtain the pose estimation with fewer optimization variables [16]. They all choose all elements of the attitude matrix as the state, which increases the computational complexity and the uncertainty of the state became complicated to obtain. In the community of aerospace, researchers prefer to choose the quaternion as a global characterization and the Rodrigues vector parameterization as a local state to track the trajectory [10]–[12], which has a concise and efficient presentation. Fosbury and Crassidis proposed relative navigation extended KF (EKF) to track the relative trajectory [13]. Whereas it needs the angular acceleration calculated using the inertial matrix of the rigid body and applied torque to propagate the state, which is impractical to realize. We instead derive a promising relative kinematic function without the angular acceleration.

This article focuses on the WSN-based relative pose estimation with some novelties. Considering an attitude matrix is locally homeomorphic to an unconstrained Lie algebra and the pairwise distances contain information of the attitude and the translation, we derive an iterative solver to estimate the pose parameterized with Lie algebra using distance measurements. The proposed solver can adopt the Gauss-Newton (GN) method or Levenberg-Marquardt (LM) method and the associated unconstrained Cramer-Rao Lower Bound (CRLB) is also derived to serve as a benchmark, which is more concise compared to the constrain CRLB [14]. We also derive a novel relative kinematic to prevent the angular acceleration and propagate the state in high accuracy with only the measurement from an IMU. The innovative kinematics formulation and the pairwise distance measurement model is introduced to the extended Kalman filter (EKF) framework to track the relative trajectory of multiple platforms. We also derive a simplified solver for rigid bodies with a degree of freedom (DOF) less than six. To show the practicability of the modified estimator, we introduce a specific application of pose estimation for the aerobridge, which only has four DOFs.

The paper is organized as follows. Section II reviews the matrix Lie group, specifically the special orthogonal group, and the associated Lie algebra. Section III derives the Jacobian matrix of the pairwise distance w.r.t. the pose for the GN and LM solver. We discuss the existence of the optimal solution in terms of sensor placement and derive the unconstrained CRLB. The innovative relative navigation of two moving rigid bodies is deduced in section IV using only the measurement of IMU and pairwise distance. The aerobridge application of the modified solver is introduced in section V.

Section VI contains three simulations. Firstly, we compare the presented solver with the q-method, the SCLS, and CLS in [14], and the proposed CRLB serves as a benchmark. Secondly, we testify the accuracy of the presented GN solver, LM solver, and the EKF. Finally, the proposed algorithm for the application of aerobridge is validated. Section VII serves as the conclusion of this article.

## II. REVIEW OF LIE GROUP AND LIE ALGEBRA

The pose of a rigid body can be parameterized using dual quaternion [18], homogeneous transformation, etc. Among these, Lie group representation is substantially used in the field of robot navigation. This section reviews the most frequently used Lie group and its homeomorphism Lie algebra, i.e. the special orthogonal group  $SO(3)$  and the equivalent rotation vector  $\mathfrak{so}(3)$  which is used to describe the attitude and its local characteristic.

A Lie group is an analytic manifold where any function on it can be expanded in a convergent Taylor series at any point [17]. The specific Lie group described in this article is the matrix Lie group whose element is represented as a squared matrix with identity matrix as identity element and the matrix multiplication and inversion are respectively the composition and inversion of the Lie group. Among the matrix Lie group,  $SO(3)$  is substantially used to describe the attitude. The definition and basic properties of  $SO(3)$  and its associated Lie algebra are presented as follows.

The  $SO(3)$  is a set of the orthogonal matrix [17], i.e.  $SO(3) = \{R \in \mathbb{R}^{3 \times 3} \mid R^T R = R R^T = I, \det R = 1\}$  representing rotation and has three degrees of freedom. An associated Lie algebra is attached to the identity element of the matrix Lie group and it describes the tangent space. It maps the element of  $SO(3)$  to a Euclidean space so that we can do differentiation. Specifically, the Lie algebra associated with  $SO(3)$  is expressed as  $\mathfrak{so}(3) = \{\Phi = \phi^\wedge \in \mathbb{R}^{3 \times 3} \mid \phi \in \mathbb{R}^3\}$ , where

$$\phi^\wedge = \begin{bmatrix} \phi_1 \\ \phi_2 \\ \phi_3 \end{bmatrix}^\wedge = \begin{bmatrix} 0 & -\phi_3 & \phi_2 \\ \phi_3 & 0 & -\phi_1 \\ -\phi_2 & \phi_1 & 0 \end{bmatrix} \quad (1)$$

is the cross product matrix and the inverse operation is  $\Phi^\vee = \phi$ . We also denote the vector  $\phi$  as Lie algebra when the context is clear. The tangent space  $\mathfrak{so}(3)$  is a vector space over the real field with the same dimensions as that of the manifold and it completely expresses the local feature at the identity. Exponential mapping associates  $SO(3)$  and  $\mathfrak{so}(3)$ , which is defined as

$$R = \exp(\phi^\wedge) = \sum_{n=0}^{\infty} \frac{1}{n!} (\phi^\wedge)^n \quad (2)$$

and the closed-form solution is the Rodrigues formulation, i.e.

$$R = \cos \phi I + (1 - \cos \phi) \mathbf{a} \mathbf{a}^T + \sin \phi \mathbf{a}^\wedge \quad (3)$$

where  $\phi = |\phi|$  and  $\mathbf{a} = \phi/\phi$ . The Lie algebra associated with  $SO(3)$  has an obvious physical significance, namely the equivalent rotation vector associated with the rotation matrix.

The global attitude of a rigid body is expressed as a nonsingular rotation matrix  $\mathbf{R}$  and the local state as an unconstrained rotation vector  $\phi$ . Because  $SO(3)$  is a topological space with a differential structure, i.e. the local charts are mutually compatible [19], we can involve  $\mathfrak{so}(3)$  in an optimization problem and iteratively obtain the optimal attitude. Generally, the local state  $\phi$  is a small quantity so it is nonsingular and functions on it can be linearized by omitting the higher-order term. We defined the perturbation form on  $SO(3)$  as

$$\mathbf{R} = \exp(\phi^\wedge) \mathbf{R}_{op} \quad (4)$$

where  $\mathbf{R}_{op}$  is the rotation on the operating point. For small angle rotation, the exponential map can be approximated by

$$\exp(\phi^\wedge) = \mathbf{I} + \phi^\wedge \quad (5)$$

where  $\mathbf{I}$  is the identity matrix. The Jacobian matrix of a vector  $\mathbf{v} \in \mathbb{R}^3$  rotated by  $\mathbf{R}$  w.r.t.  $\phi$  is [20]

$$\frac{\partial(\mathbf{R}\mathbf{v})}{\partial\phi} = -(\mathbf{R}\mathbf{v})^\wedge \quad (6)$$

which is the gradient direction and it is crucial in the following sections.

### III. POSE ESTIMATION WITH PAIRWISE DISTANCE

In this section, we present a method to estimate the relative pose of rigid bodies using pairwise distance and derive the associated covariance. Instead of estimating attitudes and translations sequentially, we obtain the optimal solution of the both simultaneously and the associated uncertainty. We exploit the unconstrained Lie algebra to construct the optimization variable, which is more efficient and superior than the CLS present in [13]. We derive the associated CRLB to numerically validate the optimality. We also discuss in which situation the optimal solution exists by considering the placement of the sensors network.

#### A. GAUSS-NEWTON SOLVER

To describe the relative pose between each pair of rigid bodies we define the body frames  $B_k (k = 1, 2, 3, \dots)$ , as shown in Fig.1. Without loss of generality, we consider estimating the relative pose of  $B_2$  w.r.t.  $B_1$ . We mount sensors on each body to measure pairwise distances. The sensors on  $B_1$  and the sensors on  $B_2$  are denoted by  $\mathbf{a}_i (i = 1, 2, 3, \dots, N)$  and  $\mathbf{b}_j (j = 1, 2, 3, \dots, M)$ , where  $N$  and  $M$  are the numbers of sensors. We denote  $\mathbf{a}_{ij}^k (\mathbf{b}_{ij}^k)$  as the coordinate vector of  $\mathbf{a}_i (\mathbf{b}_j)$  w.r.t. the frame  $B_j$  expressed in the frame  $B_k$ ,  $\mathbf{R}_i^j$  as the attitude of the frame  $B_i$  w.r.t. the frame  $B_j$  and  $\mathbf{t}_{ij}^k$  as the translation of the frame  $B_i$  w.r.t. the frame  $B_j$  expressed in the frame  $B_k$ . So, the coordinate of  $\mathbf{b}_j$  w.r.t.  $B_1$  expressed in  $B_1$  can be formulated as

$$\mathbf{b}_{j1}^1 = \mathbf{R}_2^1 \mathbf{b}_{j2}^2 + \mathbf{t}_{21}^1 \quad (7)$$

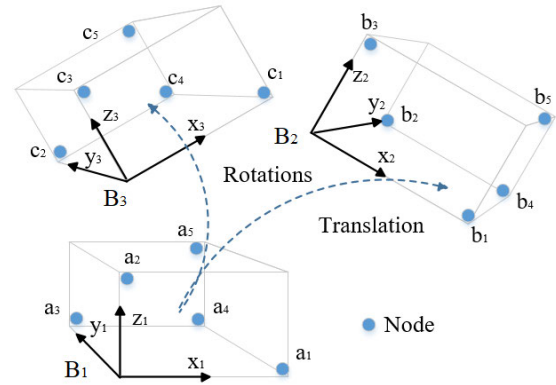


FIGURE 1. Relative motions of rigid bodies and sensors' configuration.

and the distance between  $\mathbf{a}_i$  and  $\mathbf{b}_j$  is

$$d_{ij} = \|\mathbf{a}_i - \mathbf{b}_j\| \quad (8)$$

where  $\|\cdot\|$  represents the Euclidean norm,  $\mathbf{a}_i$ , and  $\mathbf{b}_j$  are coordinate vector w.r.t. the same frame and expressed in the same frame.

Each  $\mathbf{a}_i - \mathbf{b}_j$  sensor pair from two rigid bodies can output range measurement. Generally, the measurement model is defined as

$$\tilde{d}_{ij} = \tilde{d}(\mathbf{a}_i, \mathbf{b}_j) = d_{ij} + e_{ij} \quad (9)$$

where  $e_{ij}$  is the i.i.d. zero-mean Gaussian white noise with variance  $\sigma_{ij}^2$ .

Considering (7)-(9), we can extract the pose information from range measurement. The SCLS method present in [13] uses an orthogonal projection matrix to obtain the linear function of the attitude, solve it with singular value decomposition, and further estimate the translation. It is not the optimal pose since the uncertainty of the attitude is introduced to the translation. Besides, the uncertainties of the pose estimations are not derived. We instead propose a solution based on the Gauss-Newton (GN) method to estimate the attitude and translation simultaneously without linearization and derive the covariance. Since the optimal variable is represented by Lie algebra, the complexity is mitigated and the optimization is unconstrained.

We desire to estimate the relative pose of the rigid bodies to minimize the cost function

$$\min_{\mathbf{R}, \mathbf{t}} \sum_{i,j} (\tilde{d}_{ij} - d_{ij}(\mathbf{R}, \mathbf{t}))^2, \text{ s.t. } \mathbf{R} \in SO(3) \quad (10)$$

which is a nonlinear constrained least squared (LS) optimization where  $\mathbf{R}$  is the attitude matrix and  $\mathbf{t}$  is the translation and we remove the superscript and subscript to make the equation concise. Substituting (7) in (8), we have

$$d_{ij} = \sqrt{\left( \|\mathbf{a}_i\|^2 - 2\mathbf{a}_i^T \mathbf{R} \mathbf{b}_j - 2\mathbf{a}_i^T \mathbf{t} + \|\mathbf{R} \mathbf{b}_j + \mathbf{t}\|^2 \right)} \quad (11)$$

Assuming that the global initial estimation is known and denoted as  $\mathbf{R}_{op}$  and  $\mathbf{t}_{op}$  and we define the local parameter as

$\mathbf{x} = [\Delta\boldsymbol{\phi}^T \ \Delta\mathbf{t}^T]^T$ . We expand  $d_{ij}$  with Taylor series and keep the first-order term of the local parameter as

$$d_{ij}(\Delta\boldsymbol{\phi}, \Delta\mathbf{t}) \approx d_{ij}(\mathbf{R}_{op}, \mathbf{t}_{op}) + \frac{\partial d_{ij}}{\partial \boldsymbol{\phi}} \Delta\boldsymbol{\phi} + \frac{\partial d_{ij}}{\partial \mathbf{t}} \Delta\mathbf{t} \quad (12)$$

According to (6), the derivative of distance  $d_{ij}$  w.r.t. the local parameter is

$$\frac{\partial d_{ij}}{\partial \boldsymbol{\phi}} = \frac{1}{d_{ij}} (\mathbf{R}\mathbf{b}_j)^\wedge (-\mathbf{a}_i + \mathbf{t}) \quad (13)$$

$$\frac{\partial d_{ij}}{\partial \mathbf{t}} = \frac{1}{d_{ij}} (-\mathbf{a}_i + \mathbf{R}\mathbf{b}_j + \mathbf{t}) \quad (14)$$

Consider (10) and (12), we have

$$L(\mathbf{x}) = \mathbf{z} - \mathbf{J}\mathbf{x} \quad (15)$$

where  $\mathbf{z} = \tilde{\mathbf{d}} - \mathbf{d}$  is the residual vector,  $\mathbf{d} = [d_1^T \dots d_M^T]^T \in \mathbb{R}^{NM}$ ,  $\tilde{\mathbf{d}}_j = [d_{1j} \dots d_{Nj}]^T \in \mathbb{R}^N (j = 1, \dots, M)$  and  $\mathbf{J}$  is the Jacobian matrix with the form

$$\mathbf{J} = \begin{bmatrix} \frac{\partial d_1^T}{\partial \boldsymbol{\phi}} & \dots & \frac{\partial d_M^T}{\partial \boldsymbol{\phi}} \\ \frac{\partial d_1^T}{\partial \mathbf{t}} & \dots & \frac{\partial d_M^T}{\partial \mathbf{t}} \end{bmatrix}^T \in \mathbb{R}^{NM \times 6} \quad (16)$$

So, the original constrained optimization problem is converted to calculate the local parameter  $\mathbf{x}$  so that the norm of  $L(\mathbf{x})$  is minimized, which is an unconstrained LS problem. We can solve (15) with the GN method given as

$$\mathbf{x} = -(\mathbf{J}^T \mathbf{W} \mathbf{J})^{-1} \mathbf{J}^T \mathbf{W} \mathbf{z} \quad (17)$$

where  $\mathbf{W}$  is the information matrix, i.e. the inversion of the covariance matrix of the distance observation  $\tilde{\mathbf{d}}$ .

We iteratively optimize the global estimation  $\mathbf{R}_{op} = \exp(\Delta\boldsymbol{\phi})\mathbf{R}_{op}$  and  $\mathbf{t}_{op} = \mathbf{t}_{op} + \Delta\mathbf{t}$  until the norm of  $\mathbf{x}$  convergent to a small neighbourhood of zero or the iterations reach a given number then the covariance of the estimation is

$$\mathbf{P}_x = (\mathbf{J}^T \mathbf{W} \mathbf{J})^{-1}. \quad (18)$$

Although the GN method is simple to implement, the Hessian matrix may be rank-deficient. We discuss the existence of a solution in terms of the placement of sensors in the following subsection.

### B. SOLUTION EXISTENCE AND SENSOR PLACEMENT

To ensure the optimal solution converges, the Hessian matrix  $\mathbf{H} = \mathbf{J}^T \mathbf{W} \mathbf{J}$  must be positive definite [21]. The rank of  $\mathbf{J}^T \mathbf{W} \mathbf{J}$  and  $\mathbf{J}$  are identical because they share the same null space. So, the Hessian matrix is reversible if the Jacobian matrix is column full rank, which will be ensured by configuring the sensor network topology properly.

Taking the block  $\partial d_1^T / \partial \mathbf{t}$  of Jacobian matrix in (16) into account. if we only have three independent sensors  $\mathbf{a}_i (i = 1, 2, 3)$  and  $\mathbf{b}_1$  happens to locate in the plane constructed by these  $\mathbf{a}_i$ , the block is rank deficient, which is two. It is consistent with the reason that we can not uniquely locate a moving object with three anchors using the trilateration

method. So we need one more non-coplanar sensors  $\mathbf{a}_4$  to guarantee the rank of the block is column full rank.

Next, consider the block  $\partial d_1^T / \partial \boldsymbol{\phi}$  in (16), because we have four non-coplanar sensors  $\mathbf{a}_i$ , the rank of all  $-\mathbf{a}_i + \mathbf{t}$  vectors in the block is three. But they cross product with  $\mathbf{R}\mathbf{b}_2$  cause the vectors of the block only lay on the plane perpendicular to  $\mathbf{R}\mathbf{b}_2$ . So, the rank of the block is two. Since  $\mathbf{b}_2$  and  $\mathbf{b}_3$  are independent, their perpendicular planes are not non-coplanar, Therefore the block of  $[\partial d_2^T / \partial \boldsymbol{\phi} \ \partial d_3^T / \partial \boldsymbol{\phi}]^T$  is column full rank.

To sum up, the above discussion induces that we need four non-coplanar sensors  $\mathbf{a}_i (i = 1, 2, 3, 4)$  and three independents  $\mathbf{b}_i (i = 1, 2, 3)$  to ensure the proposed solution is unique so that the algorithm is convergent. We conclude that the nonlinear optimization fit relative pose estimation perfectly with the appropriate sensor network since the Hessian matrix is always full rank in the motion

To improve the estimated accuracy, it is trivial to add one more sensor  $\mathbf{b}$ . Alternatively, we can use the trust-region methods [21], LM method for example, which can ensure higher accuracy of the estimation.

### C. CRAMER-RAO LOWER BOUND

In this subsection, we establish the unconstrained CRLB in terms of Lie algebra and translation. The proposed CRLB is more concise compare to the constrained CRB (CCRB) in [14].

Based on the measurement model described in (9), we can derive the CRLB in terms of the true Lie algebra and translation, which serves as a benchmark to numerically validate the optimality of the proposed method. The covariance of the unbiased estimate  $\mathbf{x}$  satisfies

$$\mathbf{E} \{ (\hat{\mathbf{x}} - \mathbf{x})(\hat{\mathbf{x}} - \mathbf{x})^T \} \geq \mathbf{F}^{-1} \quad (19)$$

where  $\mathbf{A} \geq \mathbf{B}$  means  $\mathbf{A} - \mathbf{B}$  is a positive semidefinite and  $\mathbf{E} \{ \cdot \}$  denotes the expectation operation.  $\mathbf{F}$  is the Fisher information matrix defined as

$$\begin{aligned} \mathbf{F} &= \sum_{i=1}^N \sum_{j=1}^M \mathbf{E} \left\{ \frac{\partial \ln p(\tilde{d}_{ij}; \mathbf{x})}{\partial \mathbf{x}} \frac{\partial \ln p(\tilde{d}_{ij}; \mathbf{x})}{\partial \mathbf{x}^T} \right\} \\ &= \sum_{i=1}^N \sum_{j=1}^M \mathbf{F}_{ij}, \end{aligned} \quad (20)$$

where the probability distribution function (PDF) of the range measurement is given as

$$p(\tilde{d}_{ij}; \mathbf{x}) = \frac{1}{\sqrt{2\pi}\sigma_{ij}} \exp\left(-\frac{(\tilde{d}_{ij} - d_{ij})^2}{2\sigma_{ij}^2}\right) \quad (21)$$

Taking the first partial derivative of  $\ln p(\tilde{d}_{ij}; \mathbf{x})$  w.r.t.  $\mathbf{x}$  yields

$$\frac{\partial \ln p(\tilde{d}_{ij}; \mathbf{x})}{\partial \mathbf{x}} = \frac{(\tilde{d}_{ij} - d_{ij})}{\sigma_{ij}^2} \frac{\partial d_{ij}}{\partial \mathbf{x}} \quad (22)$$



Taking the expectation operation gives

$$\mathbf{F}_{ij} = \frac{1}{\sigma_{ij}^2} \frac{\partial d_{ij}}{\partial \mathbf{x}} \frac{\partial d_{ij}}{\partial \mathbf{x}^T} \quad (23)$$

where the partial derivative is given in (15) and (16).

According to the theorem 2 in [13], any attitude estimator is biased for its highly nonlinear feature. The bias increases as the measurement noises get noisy and the mean-squared-error (MSE) of any attitude estimator will be lower than the CRLB for high noise levels. Although we choose unconstrained Lie algebra as the state, its norm is restricted to between 0 to  $2\pi$ . So the saturate situation state above will still appear. However, at low noise levels, the bias tends to zero, and the CRLB still can serve as a reference to measure the optimality of the estimator.

#### IV. NOVEL EKF DESIGN FOR TRACKING RELATIVE POSE

In this section, we design an EKF incorporating inertial measurements and pairwise distances to estimate the state of relative navigation including relative pose and relative velocity of the leader w.r.t. the follower and biases of the gyroscope and accelerometer on the follower. The Jacobian matrix derived in section III are used as the sensitivity matrix in the measurement update phase. With IMU measurement, the estimated relative pose are smoother than that of GN and LM solver. The propagated process here and those in [13] differ in the relative angular acceleration which is untrivial to accurately obtain. In [13], the inertial matrix of the body and the applied torque have to be known to calculate the relative angular acceleration using the Euler equation. Generally, the applied torque can be imprecise and the inertial matrix can change as the load or the shape of the body change, so it is difficult to achieve the precise relative angular acceleration in most vehicles. We instead get rid of the term without adding other measurements and the performance is at least as good as that of [13].

We now introduce the measurement model of the IMU, which can generate linear acceleration and angular velocity. The output signals are usually corrupted with noise, drifts, and biases. For the inertial measurement of follower, the measurement model of the accelerometer is defined as [10]

$$\begin{aligned} \tilde{\mathbf{a}}_f^i &= \mathbf{R}_i^f \left( \ddot{\mathbf{i}}_{f|i}^i + \mathbf{g}^i \right) + \boldsymbol{\beta}_a + \boldsymbol{\eta}_{av} \\ &= \mathbf{a}_f^i + \boldsymbol{\beta}_a + \boldsymbol{\eta}_{av} \end{aligned} \quad (24)$$

$$\dot{\boldsymbol{\beta}}_a = \boldsymbol{\eta}_{au} \quad (25)$$

where  $\ddot{\mathbf{i}}_{f|i}^i$  is the linear acceleration vector of the follower w.r.t. the initial origin expressed in the inertial frame,  $\mathbf{g}$  is the gravity,  $\boldsymbol{\beta}_a$  is the bias,  $\boldsymbol{\eta}_{av}$  and  $\boldsymbol{\eta}_{au}$  are supposed to be i.i.d. zero-mean white random processes with variances  $\sigma_{av}^2 \mathbf{I}_{3 \times 3}$  and  $\sigma_{au}^2 \mathbf{I}_{3 \times 3}$ . It is noted that the boldfaced  $\mathbf{a}$  standards for linear acceleration instead of coordinate vector in this section.

The measurement of the gyroscope has a similar model:

$$\tilde{\boldsymbol{\omega}}_f^i = \boldsymbol{\omega}_f^i + \boldsymbol{\beta}_g + \boldsymbol{\eta}_{gv} \quad (26)$$

$$\dot{\boldsymbol{\beta}}_g = \boldsymbol{\eta}_{gu} \quad (27)$$

where  $\boldsymbol{\beta}_g$  is the gyro bias,  $\boldsymbol{\eta}_{gv}$  and  $\boldsymbol{\eta}_{gu}$  are i.i.d. zero-mean white random processes with variances  $\sigma_{gv}^2 \mathbf{I}_{3 \times 3}$  and  $\sigma_{gu}^2 \mathbf{I}_{3 \times 3}$ . For the IMU mounted in the leader, the accelerometer and gyro measurement are assumed to be known precisely.

Assuming that the state of absolute navigation of the leader can be precisely obtained in advance, the state of interest in relative navigation is the relative attitude  $\mathbf{R}_l^f$ , relative position  $\mathbf{t}_{l|f}^f$  and relative velocity  $\dot{\mathbf{t}}_{l|f}^f$  of the leader w.r.t. the follower and biases on the inertial acceleration  $\boldsymbol{\beta}_a$  and angular velocity measurements  $\boldsymbol{\beta}_g$ . We propose a different propagation process in the following.

Defining  $\mathbf{R}_{f,k}^+$  ( $\mathbf{R}_{l,k}^+$ ) move the attitude of the follower (leader) at time  $k$  to next moment the discrete propagation of the attitude is

$$\mathbf{R}_{l,k+1}^f = \mathbf{R}_{f,k}^+ \mathbf{R}_{l,k}^f \mathbf{R}_{l,k}^{+T} \quad (28)$$

where

$$\mathbf{R}_{f,k}^+ = \exp\left(-\boldsymbol{\omega}_{f,k}^f \wedge T\right), \mathbf{R}_{l,k}^+ = \exp\left(-\boldsymbol{\omega}_{l,k}^l \wedge T\right) \quad (29)$$

Consider the equation

$$\mathbf{t}_{l|f}^f = \mathbf{R}_i^f \mathbf{t}_{l|f}^i \quad (30)$$

$$\mathbf{R}_i^f \dot{\mathbf{t}}_{l|f}^i = \dot{\mathbf{t}}_{l|f}^f + \boldsymbol{\omega}_f^f \wedge \mathbf{t}_{l|f}^f \quad (31)$$

$$\begin{aligned} \mathbf{t}_{l|f,k+1}^i &= \mathbf{t}_{l|f,k}^i + \dot{\mathbf{t}}_{l|f,k}^i T \\ &\quad + 0.5 \times \left( \ddot{\mathbf{t}}_{l|i,k}^i - \ddot{\mathbf{t}}_{f|i,k}^i \right) T^2 \end{aligned} \quad (32)$$

where  $T$  is the sampling duration and the superscribe  $i$  standard for the inertial frame, the propagation of the translation can be derived as

$$\begin{aligned} \mathbf{t}_{l|f,k+1}^f &= \mathbf{R}_{f,k}^+ \left[ \left( \mathbf{I} + \boldsymbol{\omega}_{f,k}^f \wedge T \right) \mathbf{t}_{l|f,k}^f + \dot{\mathbf{t}}_{l|f,k}^f T \right. \\ &\quad \left. + 0.5 \times \left( \mathbf{R}_{l,k}^f \mathbf{a}_{l,k}^l - \mathbf{a}_{f,k}^f \right) T^2 \right] \end{aligned} \quad (33)$$

where we assume the follower and the leader are relatively close and the gravity term vanishes. Based upon (31)-(33), along with the equation

$$\mathbf{R}_{i,k}^f \dot{\mathbf{t}}_{l|f,k+1}^i = \mathbf{R}_{i,k}^f \dot{\mathbf{t}}_{l|f,k}^i + \left( \mathbf{R}_{l,k}^f \mathbf{a}_{l,k}^l - \mathbf{a}_{f,k}^f \right) T \quad (34)$$

$$\mathbf{R}_{f,k}^+ \boldsymbol{\omega}_{f,k}^f = \boldsymbol{\omega}_{f,k}^f \wedge \mathbf{R}_{f,k}^+ \quad (35)$$

the propagation of the velocity is

$$\begin{aligned} \dot{\mathbf{t}}_{l|f,k+1}^f &= \left( \mathbf{I} - \boldsymbol{\omega}_{f,k+1}^f \wedge \right) \mathbf{R}_{f,k}^+ \dot{\mathbf{t}}_{l|f}^f \\ &\quad + \left( \boldsymbol{\omega}_{f,k}^f \wedge - \boldsymbol{\omega}_{f,k+1}^f \wedge - \boldsymbol{\omega}_{f,k+1}^f \wedge \boldsymbol{\omega}_{f,k}^f \wedge T \right) \mathbf{R}_{f,k}^+ \mathbf{t}_{f|i,k}^f \\ &\quad + \left( \mathbf{I} - 0.5 \times T \boldsymbol{\omega}_{f,k+1}^f \wedge \right) \mathbf{R}_{f,k}^+ \left( \mathbf{R}_{l,k}^f \mathbf{a}_{l,k}^l - \mathbf{a}_{f,k}^f \right) T \end{aligned} \quad (36)$$

The propagation of the bias is identical with [13]. Using the above presentation, it is unnecessary to calculate the angular acceleration, which is more practical to implement and the estimated state is more accurate. To keep this article concise, in the following derivation we vanish the  $f$  and  $l$  in the subscribe and superscripted for the state of interest and the

inertial measurement of the follower, i.e.  $\mathbf{R} = \mathbf{R}_l^f$ ,  $\mathbf{t} = \mathbf{t}_{lf}^f$ ,  $\dot{\mathbf{t}} = \dot{\mathbf{t}}_{lf}^f$ ,  $\boldsymbol{\omega} = \boldsymbol{\omega}_f^f$  and  $\mathbf{a} = \mathbf{a}_f^f$  and denote  $\mathbf{R}_f^+$  as  $\mathbf{R}^+$ . Based on the truth equations (28), (29), (33), and (36) and considering

$$\hat{\boldsymbol{\omega}}_k = \tilde{\boldsymbol{\omega}}_k - \hat{\boldsymbol{\beta}}_{g,k}, \hat{\boldsymbol{\omega}}_{k+1} = \tilde{\boldsymbol{\omega}}_{k+1} - \hat{\boldsymbol{\beta}}_{g,k}, \hat{\mathbf{a}}_k = \tilde{\mathbf{a}}_k - \hat{\boldsymbol{\beta}}_{a,k} \quad (37)$$

$$\hat{\boldsymbol{\beta}}_{a,k+1} = \hat{\boldsymbol{\beta}}_{a,k}, \hat{\boldsymbol{\beta}}_{g,k+1} = \hat{\boldsymbol{\beta}}_{g,k} \quad (38)$$

the state of interest can be propagated, where the bias is assumed to be unchanged during the interval for simplicity. Our next step involves the propagation of the covariance. The error state of the EKF is chosen as

$$\Delta \mathbf{x} = \begin{bmatrix} \Delta \boldsymbol{\phi}^T & \Delta \mathbf{t}^T & \Delta \dot{\mathbf{t}}^T & \Delta \boldsymbol{\beta}_g^T & \Delta \boldsymbol{\beta}_a^T \end{bmatrix}^T \quad (39)$$

where  $\Delta \boldsymbol{\phi}$  is the small angle error of the relative attitude with its estimation defined as

$$\Delta \boldsymbol{\phi} = \left( \mathbf{R} \hat{\mathbf{R}}^T \right)^\vee \quad (40)$$

The remaining state-error terms are defined generically as  $\Delta \mathbf{y} = \mathbf{y} - \hat{\mathbf{y}}$ . To propagate the covariance, we derive the discrete kinematics of the error, i.e.

$$\Delta \mathbf{x}_{k+1} = \mathbf{F}_k \Delta \mathbf{x}_k + \mathbf{G}_k \mathbf{n}_k \quad (41)$$

where the process noise vector consists of the Gaussian noise terms from the inertial measurement equations is

$$\mathbf{n}_k = \begin{bmatrix} \eta_{gv,k}^T & \eta_{gv,k+1}^T & \eta_{\alpha v,k}^T & \eta_{gu,k}^T & \eta_{au,k}^T \end{bmatrix}^T \quad (42)$$

where  $\eta_{gv,k+1}$  is introduced from  $\boldsymbol{\omega}_{f,k+1}^f$  in (36). Make use of the prior propagation equation already mention above and omit the algebra derivation, the final results are given as

$$\mathbf{F} = \begin{bmatrix} \hat{\mathbf{R}}_k^+ & \mathbf{0}_{3 \times 3} & \mathbf{0}_{3 \times 3} & \mathbf{TI}_{3 \times 3} & \mathbf{0}_{3 \times 3} \\ \mathbf{F}_{21} & \mathbf{F}_{22} & \hat{\mathbf{R}}_k^+ \mathbf{T} & \mathbf{F}_{24} & 0.5 \hat{\mathbf{R}}_k^+ \mathbf{T}^2 \\ \mathbf{F}_{31} & \mathbf{F}_{32} & \mathbf{F}_{33} & \mathbf{F}_{34} & \mathbf{F}_{35} \\ \mathbf{0}_{3 \times 3} & \mathbf{0}_{3 \times 3} & \mathbf{0}_{3 \times 3} & \mathbf{I}_{3 \times 3} & \mathbf{0}_{3 \times 3} \\ \mathbf{0}_{3 \times 3} & \mathbf{0}_{3 \times 3} & \mathbf{0}_{3 \times 3} & \mathbf{0}_{3 \times 3} & \mathbf{I}_{3 \times 3} \end{bmatrix} \quad (43)$$

$$\mathbf{G} = \begin{bmatrix} \mathbf{TI}_{3 \times 3} & \mathbf{0}_{3 \times 3} & \mathbf{0}_{3 \times 3} & \mathbf{0}_{3 \times 3} & \mathbf{0}_{3 \times 3} \\ \mathbf{G}_{21} & \mathbf{0}_{3 \times 3} & 0.5 \hat{\mathbf{R}}_k^+ \mathbf{T}^2 & \mathbf{0}_{3 \times 3} & \mathbf{0}_{3 \times 3} \\ \mathbf{G}_{31} & \mathbf{G}_{32} & \mathbf{G}_{33} & \mathbf{0}_{3 \times 3} & \mathbf{0}_{3 \times 3} \\ \mathbf{0}_{3 \times 3} & \mathbf{0}_{3 \times 3} & \mathbf{0}_{3 \times 3} & \mathbf{TI}_{3 \times 3} & \mathbf{0}_{3 \times 3} \\ \mathbf{0}_{3 \times 3} & \mathbf{0}_{3 \times 3} & \mathbf{0}_{3 \times 3} & \mathbf{0}_{3 \times 3} & \mathbf{TI}_{3 \times 3} \end{bmatrix} \quad (44)$$

where the general EKF assumption is that the estimate is close, to within first-order dominant terms, to the truth is applied. To keep this article concise, we left some lengthy elements in appendix A. We further derive the update process of the EKF. The observation equation is defined as

$$\tilde{d}_{ij,k} = d_{ij,k}(\mathbf{R}, \mathbf{t}) + v_{ij,k} \quad (45)$$

where  $v_{ij,k}$  is a zero-mean Gaussian white noise with a known variance. We can derive the measurement sensitivity matrix as

$$\mathbf{h}_{ij,k} = \begin{bmatrix} \frac{\partial d_{ij,k}}{\partial (\Delta \boldsymbol{\phi}^T)} & \frac{\partial d_{ij,k}}{\partial (\Delta \mathbf{t}^T)} & \mathbf{0}_{1 \times 3} & \mathbf{0}_{1 \times 3} & \mathbf{0}_{1 \times 3} \end{bmatrix} \quad (46)$$

Based on (12)-(14), the presentation in detail can be evaluated. Then the update process is performed using the residual. If more than one distance measurement is available, we can stack the observation to obtain estimation with higher precision. The Kalman gain computation and covariance update have the standard Kalman filter forms.

## V. APPLICATION ON AEROBRIDGE

In section III, we present relative pose estimators based on pairwise distance measurement and discuss the existence of the solution. We can apply the nonlinear optimization to rigid bodies with six degrees of freedom (DOF) (three for attitude and three for translation). For rigid bodies with less DOF, we care about the minimum amount of sensors to ensure a convergent solution, because the sampling period of a WSN drops rapidly with an additional sensor.

Specifically, we consider the aeroBridge (connector between an airplane and a terminal building) with only four DOF in Fig. 2 whose 3D model is shown in Fig. 3. Since the expensive labor force facilitates its autopilot, it attracts attention recently.



FIGURE 2. An aeroBridge manufactured by CIMC Tianda Holdings Co., Ltd.

We desire to estimate the attitude and position of end effector w.r.t. the terminal building, i.e. the pose of the body frame  $B$  w.r.t. the inertial frame  $I$ . To select the estimated variable, we analyze the mechanical structure below. We have three revolute joints denoted as  $a_i (i = 1, 2, 3)$  where  $a_3$  is an equivalent revolute joint. The end effector rotated around  $a_3$  when it is elevated and descended. Besides, we have a prismatic joint denoted as  $l_2$  which can extend and retract. The remainder  $l_1$  and  $l_3$  are the rigid links. Based on the analysis above, the aeroBridge has only four DOF.

We can configure four nodes on the terminal building and three on the end effector and estimated the pose with the algorithm described in section III. Alternatively, we can instead estimate the joint parameters and use forward kinematic to calculated the pose. With less estimated variables, the later requires less information to guarantee a convergent solution. So, we prefer to estimate the joint parameters. Because the end effector is always in front of the terminal building,

we allocation three anchors (sensors with fixed position)  $A_i(i = 1, 2, 3)$  on the building and two sensors  $M_j(j = 1, 2)$  on the aerobridge (one on the end effector and the other on the axis  $a_2$ ), as shown in Fig.3.

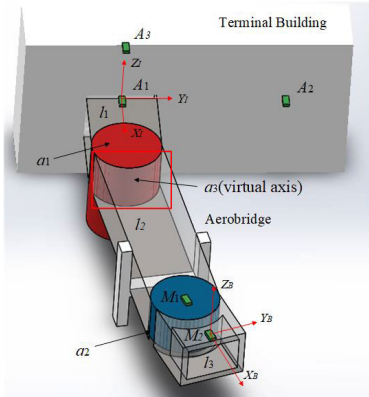


FIGURE 3. The three-dimension model of an aerobridge.

To use the algorithm framework presented in section III, we derive the Jacobian matrix of the distances w.r.t. the joints parameters. We use Denavit-Hartenberg (DH) parameterization to construct the aerobridge model, as shown in Fig. 4 and the DH parameters are shown in table 1. We want to estimate the joint variable which is defined as  $\mathbf{x} = [\theta_1 \ \theta_2 \ d_3 \ \theta_4]^T$ .

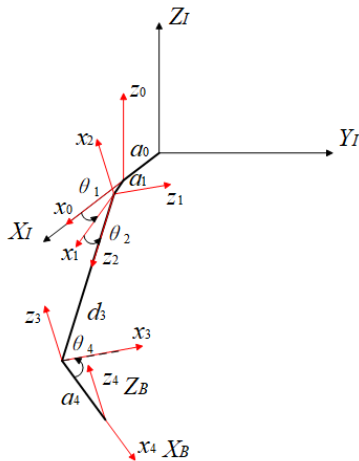


FIGURE 4. The DH parametric model of the aerobridge.

TABLE 1. DH parameter of the aerobridge.

link	$\theta$	$\alpha$	$a$	$d$
0 - 1	$\theta_1(0)$	$-\pi/2$	$a_1$	0
1 - 2	$\theta_2(-\pi/2)$	$-\pi/2$	0	0
2 - 3	$-\pi/2$	$-\pi/2$	0	$d_3(20)$
3 - 4	$\theta_4(-\pi/2)$	0	$a_4$	0

As Fig. 4 shows, the mobile sensors  $M_1$  and  $M_2$  is located on the origin of frame 3 and 4. The coordinate of  $M_j(j = 1, 2)$

in terms of the joint variables is given as

$$\mathbf{b}_{1|l}^I = \begin{bmatrix} -d_3c_1s_2 + a_1c_1 \\ -d_3s_1s_2 + a_1s_1 \\ -d_3c_2 \end{bmatrix} \quad (47)$$

$$\mathbf{b}_{2|l}^I = \begin{bmatrix} a_4(c_1s_2s_4 - s_1c_4) - d_3c_1s_2 + a_1c_1 \\ a_4(s_1s_2s_4 + c_1c_4) - d_3s_1s_2 + a_1s_1 \\ a_4c_2s_4 - d_3c_2 \end{bmatrix} \quad (48)$$

where the superscript and subscript follow the definition in section III and  $s_i$  ( $c_i$ ) stands for  $\sin\theta_i$  ( $\cos\theta_i$ ). Reformulate (10) as

$$d_{ij} = \|\mathbf{a}_{i|l}^I - \mathbf{b}_{j|l}^I\| \quad (49)$$

where  $\mathbf{a}_{i|l}^I$  is the coordinate of  $A_i$ . Consider (47) and (48), the partial derivative of distance  $d_{ij}$  w.r.t. the joint vector  $\mathbf{x}$  is given as

$$J_{ij} = \frac{\partial d_{ij}}{\partial \mathbf{x}^T} = \begin{bmatrix} \frac{\partial d_{ij}}{\partial \theta_1} & \frac{\partial d_{ij}}{\partial \theta_2} & \frac{\partial d_{ij}}{\partial d_3} & \frac{\partial d_{ij}}{\partial \theta_4} \end{bmatrix} \quad (50)$$

where the mathematical calculation is left in the appendix B. According to (15) and (17), we construct the residual and Jacobian matrix to iteratively calculate the local joint variables until the loss function reaches a given threshold. The covariance matrix  $P_J$  of the joint vector is calculated with (18).

The next step involves the propagation from joint variables to the pose of the end effector and the associated covariance using forward kinematic. Consider the DH parametric model, the relationship between attitude and joint variables can be expressed using a rotation matrix, i.e.

$$R(\mathbf{x}) = \begin{bmatrix} c_1s_2s_4 - s_1c_4 & c_1s_2c_4 + s_1s_4 & c_1c_2 \\ s_1s_2s_4 + c_1c_4 & s_1s_2c_4 - c_1s_4 & s_1c_2 \\ c_2s_4 & c_2c_4 & -s_2 \end{bmatrix} \quad (51)$$

Introducing the error of joint variables, we have

$$R(\mathbf{x} + \Delta\mathbf{x}) = R(\mathbf{x}) + \Delta R_A \quad (52)$$

where  $\Delta\mathbf{x} = [\Delta\theta_1 \ \Delta\theta_2 \ \Delta d_3 \ \Delta\theta_4]^T$ , the additive error rotation matrix is

$$\Delta R_A = \begin{bmatrix} r_{11} & r_{12} & -s_1c_2\Delta\theta_1 - c_1s_2\Delta\theta_2 \\ r_{21} & r_{22} & c_1c_2\Delta\theta_1 - s_1s_2\Delta\theta_2 \\ r_{31} & r_{32} & -c_2\Delta\theta_2 \end{bmatrix} \quad (53)$$

$$r_{11} = (-s_1s_2s_4 - c_1c_4) \Delta\theta_1 + c_1c_2s_4 \Delta\theta_2 + (c_1s_2c_4 + s_1s_4) \Delta\theta_4 \quad (54)$$

$$r_{12} = (-s_1s_2c_4 + c_1s_4) \Delta\theta_1 + c_1c_2c_4 \Delta\theta_2 - (c_1s_2s_4 + s_1c_4) \Delta\theta_4 \quad (55)$$

$$r_{21} = (c_1s_2s_4 - s_1c_4) \Delta\theta_1 + s_1c_2s_4 \Delta\theta_2 + (s_1s_2c_4 - c_1s_4) \Delta\theta_4 \quad (56)$$

$$r_{22} = (c_1s_2c_4 + s_1s_4) \Delta\theta_1 + s_1c_2c_4 \Delta\theta_2 - (s_1s_2s_4 + c_1c_4) \Delta\theta_4 \quad (57)$$

$$r_{31} = -s_2s_4 \Delta\theta_2 + c_2c_4 \Delta\theta_4 \quad (58)$$

$$r_{32} = -s_2c_4 \Delta\theta_2 - c_2s_4 \Delta\theta_4 \quad (59)$$

We used the GN method to estimate the joint variable above and the uncertainty is additive. To maintain normalized attitude, MEKF (multiplicative EKF) uses multiplicative attitude errors to update the state and its performance is generally better than additive EKF because artificial normalization will introduce additional errors. To introduce attitude observation into MEKF, we need to convert the above-mentioned attitude additive error into multiplicative error. Define the multiplicative error expressed as

$$\begin{aligned} \Delta R_M &= R^{-1}(x)R(x + \Delta x) \\ &= \exp(\Delta\phi^\wedge) \\ &\approx I + \Delta\phi^\wedge \end{aligned} \quad (60)$$

where Lie algebra is used to represent the multiplicative error rotation matrix, and the first-order term is retained. So, substitute (29) into (35), and the Lie algebra corresponding to the multiplicative error is

$$\Delta\phi = \left(R^{-1}(x)\Delta R_A\right)^\vee = F_{RJ}\Delta x \quad (61)$$

where  $F_{RJ}$  represents the transfer matrix from joint error to multiplicative attitude error, omits the complicated calculation process, and directly gives the expression of  $F_{RJ}$  as

$$F_{RJ} = \begin{bmatrix} -c_1s_4 & c_4 & 0 & 0 \\ c_2c_4 & -s_4 & 0 & 0 \\ -s_2 & 0 & 0 & 1 \end{bmatrix} \quad (62)$$

So the covariance of the multiplicative attitude error is

$$P_R = F_{RJ}P_JF_{RJ}^T \quad (63)$$

For position estimation, consider the position vector expression in forward kinematics, i.e. (48), define the position error as

$$\Delta t = t(x + \Delta x) - t(x) \quad (64)$$

Omitting the complicated mathematics process, the transfer relationship between the position error and the joint variable error is directly obtained as

$$\Delta t = F_{TJ}\Delta x \quad (65)$$

where

$$F_{TJ} = \begin{bmatrix} f_{11} & f_{12} & -c_1s_2 & f_{14} \\ f_{21} & f_{22} & -s_1s_2 & f_{24} \\ 0 & f_{32} & -c_2 & a_4c_2c_4 \end{bmatrix} \quad (66)$$

$$f_{11} = -a_4(s_1s_2s_4 + c_1c_4) + d_3s_1s_2 - a_1s_1 \quad (67)$$

$$f_{12} = a_4c_1c_2s_4 - d_3c_1c_2 \quad (68)$$

$$f_{14} = a_4(c_1s_2c_4 + s_1s_4) \quad (69)$$

$$f_{21} = a_4(c_1s_2s_4 - s_1c_4) - d_3c_1s_2 + a_1c_1 \quad (70)$$

$$f_{22} = a_4s_1c_2s_4 - d_3s_1c_2 \quad (71)$$

$$f_{24} = a_4(s_1s_2c_4 - c_1s_4) \quad (72)$$

$$f_{32} = -a_4s_2s_4 + d_3s_2 \quad (73)$$

So the covariance of the translation error is

$$P_T = F_{TJ}P_JF_{TJ}^T \quad (74)$$

## VI. EXPERIMENT VALIDATION

In this section, we design three simulations to verify the performance of the proposed method. We compare the presented GN estimator, denoted as LLS estimator since it uses Lie algebra to parameterize the LS problem, with the simplified unitarily constrained LS (SCLS) estimator, the unitarily constrained LS (CLS) estimator [13], and the q-method [9] in a stationary scenario and using CRLB as a benchmark. Then we track the relative pose between two moving rigid bodies using the proposed GN estimator, LM estimator, and EKF. Finally, we validate the modified LS method using in the moving aerobridge. All simulation is performed in MATLAB using the Robotics Toolbox maintained by Peter Corke.

### A. COMPARISON OF STEADY-STATE ACCURACY

To illustrate the superiority of the proposed LLS estimator, we set the coordinates of sensors and anchors as that of [14], i.e.

$$C = \begin{bmatrix} 0.5 & 1.5 & 1.5 & 0.5 & 1 \\ 0 & 0 & 1.5 & 1.5 & 1 \\ 0 & 0 & 0 & 0 & 1 \end{bmatrix} \text{ m} \quad (75)$$

$$A = \begin{bmatrix} 0 & 100 & 0 & 100 \\ 100 & 100 & 0 & 0 \\ 0 & 100 & 100 & 0 \end{bmatrix} \quad (76)$$

We parameterize the attitude by Euler angle  $\phi = [20 \ -25 \ 10]^T$  deg in the sequence of XYZ and the translation is  $t = [15 \ 5 \ 10]^T$  m. We use q-method to initialize CLS and LLS. The simulations are averaged over  $N_{\text{exp}} = 1000$  independent Monte-Carlo experiments with different measurement deviation  $\sigma$ . We utilize the bias, the root-mean-squared-error (RMSE), and the associated CCRB defined in [14] to analyze the precision. The comparisons shown in Fig. 5 and Fig. 6 illustrate the proposed method has a smaller bias and the RMSE meets the CCRB in a large range of noise deviation.

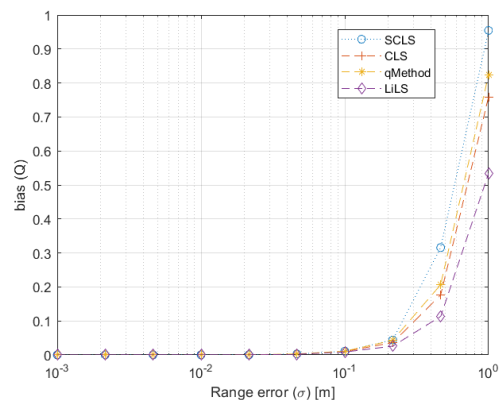


FIGURE 5. The bias of the estimated attitude.



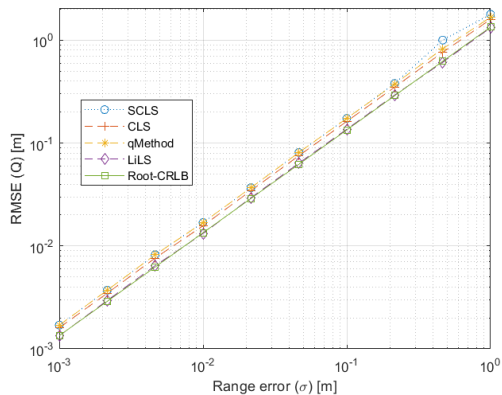


FIGURE 6. The RMSE of the estimated attitude.

We also define RMSE for the small rotation perturbation as

$$RMSE(\phi) = \left( \frac{1}{N_{exp}} \sum_{n=1}^{N_{exp}} \|\phi\|^2 \right)^{1/2} \quad (77)$$

where  $\phi$  is defined as

$$\phi = \ln(R\hat{R}^T) \quad (78)$$

and  $\ln(\cdot)$  is the logarithm mapping Lie group to Lie algebra. We draw in Fig. 7 the RMSE of  $\phi$  and the associated CRLB defined in (21). The performance is consistent with Fig. 6 that the proposed estimator has higher precision.

The SCLS estimator diverges when the number of sensors is less than four because the matrix operated by SVD is rank deficient while other estimators can still work except for slightly degraded precision, which is shown in Fig. 8.

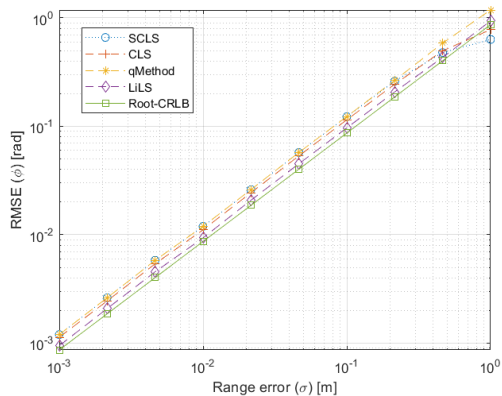


FIGURE 7. The RMSE of the estimated attitude in term of rotated perturbation.

The bias and RMSE of the estimated translation are shown in Fig. 9 and Fig. 10 from which we can see the bias of the LLS estimator is smaller and the precision can meet the CCRB. It is a quite general result that the CRLB always increases as we estimate more parameters [22], so the CRLB of a translation calculated using the LLS estimator is lower than the CCRB.

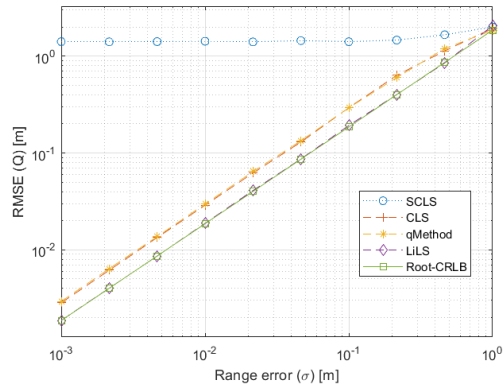


FIGURE 8. RMSE of attitude with 3 sensors.

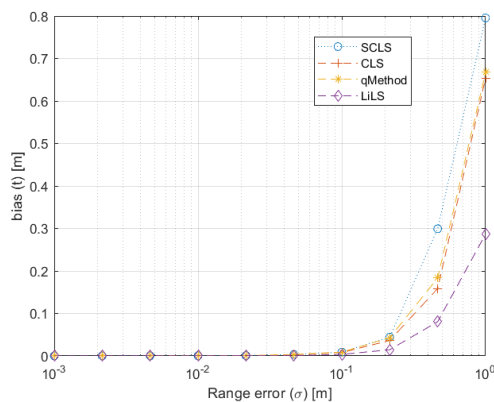


FIGURE 9. The bias of the estimated translation.

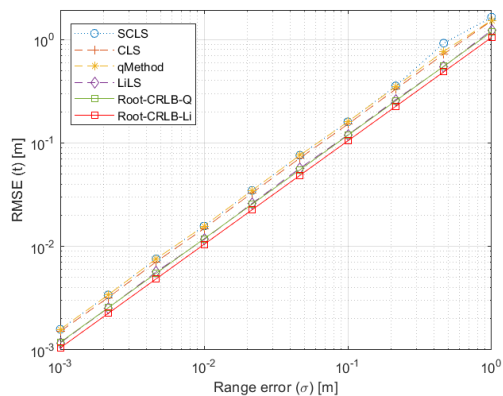


FIGURE 10. The bias and RMSE of the estimated translation.

### B. TRACKING THE RELATIVE POSE OF TWO MOVING RIGID BODIES

In this subsection, the docking process of two moving rigid bodies, namely the leader L and the follower F, is simulated based on Robotics Toolbox. To ensure that the algorithm is repeatable and robust, we do 100 independent Monte-Carlo experiments. The initial positions of both are uniformly distributed inside a cube with 10m length in the seventh and first hexagram limits of the inertial frame. The initial attitudes parameterized by Euler angles are uniformly distributed

between 0 to  $\pi$  along each axis. The final attitude coincides with the inertial frame and their position are respectively  $t_L = [0 \ 0 \ 0]^T$  and  $t_F = [0 \ 0 \ 2]^T$ . We sequentially perform the presented GN solver, LM solver, and EKF to compare the performance. We have discussed the existence of solutions in terms of the rank of the Hessian matrix in subsection III-B and we draw a conclusion that to ensure a global convergence with any initial state, four sensors are necessary. We choose the topology of the sensors in each body as

$$S_L = S_F = \begin{bmatrix} 1 & 0 & 0 & 1 \\ 0 & 1 & 0 & 1 \\ 0 & 0 & 1 & 1 \end{bmatrix} m \quad (79)$$

The standard deviation of range measurement is 0.01m, which is common for UWB devices, e.g. the P440 of the Time Domain company [24]. The pose estimation is initialized by the linearization process and q-method [9].

One challenging instance of the experiments is shown in Fig. 11 and the trajectory of the relative pose is illustrated in Fig. 12. The initial relative attitude is  $\varphi_0 = [176.04 \ 5.09 \ -60.23]^T$  deg in ZYX order and the translation is  $t_0 = [-14.99 \ -15.43 \ 7.05]^T$  m. The distance of the both is 22.64m while the sensors have only 1m separation.

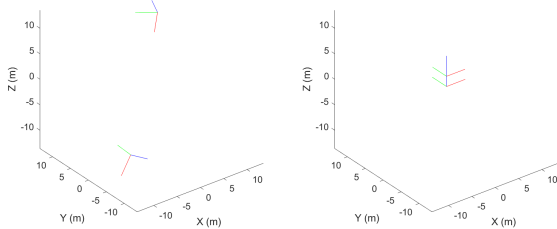


FIGURE 11. Docking process of two rigid bodies.

The errors of the relative attitude and translation estimated by GN and LM solver are shown in Fig. 13 and Fig. 14, where the error of attitude is presented by small rotation perturbation in (72). The envelope dotted curve is the  $3\sigma$  boundary calculate with (20). The red dash curve is the error of the GN estimator and the black solid curve is the error of the LM estimator. The initial pose errors are large since two bodies are far from each other initially, but the errors are mitigated as two bodies get close. It is alternatively to enlarge the distances of the sensors to alleviate the error, which is intuitively similar to trilateration [25]. We find the GN estimator outperforms the GPS and it is globally convergent while the LM estimator can almost reach under 10cm and several degrees accuracy for relative translation and attitude.

Although the accuracy of the LM estimator is greatly higher than the GN estimator, the maximum errors of attitude and translation are beyond 1deg and 10cm respectively. It may be sufficiently precise for some scenarios but it is possible to improve the performance with IMU measurement. Besides, with four sensors mounted on each body, the LM and GN estimator can obtain global convergence but measuring all pairwise distances can be time-consuming. When

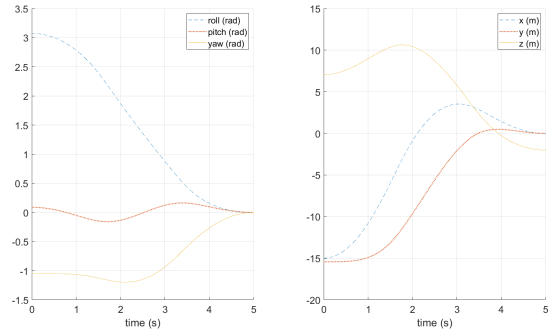


FIGURE 12. The trajectory of the relative pose.

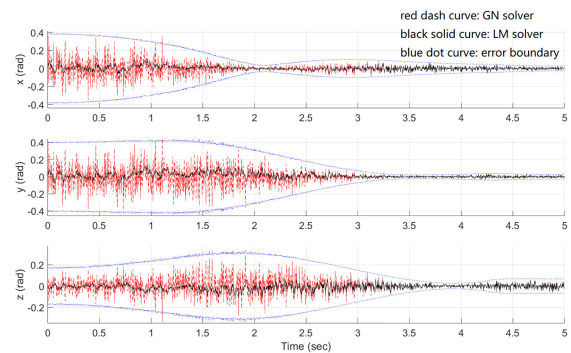


FIGURE 13. The attitude error of the GN and LM estimator and  $3\sigma$  boundary.

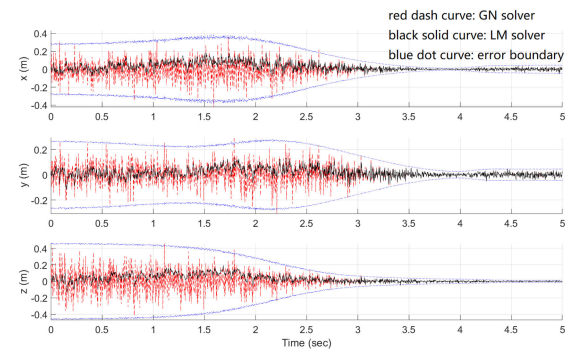


FIGURE 14. The translation error of the GN and LM estimator and  $3\sigma$  boundary.

only three sensors are mounted on each body and the plane constructed by the three sensors are parallel, two relative translations satisfy the distance measurement so the error is divergent. If the relative velocities are known, we can obtain a unique solution. Based on the idea, we used three sensors and one IMU on each body to perform the presented EKF. To be practical, the parameter of the IMU chosen in Table 2 is considerably large and common in civilian equipment.

The performance of the EKF shown in Fig. 15 and Fig. 16 are globally convergent in the Monte-Carlo experiments with different initial poses. We also add the case of mounting four

TABLE 2. IMU Noise Parameters.

Gyro Noise	$\sigma_{gv} = 7 \times 10^{-4} [\text{rad}/(s\sqrt{\text{Hz}})]$ $\sigma_{gu} = 4 \times 10^{-4} [\text{rad}/(s^2\sqrt{\text{Hz}})]$
Accelerometer Noise	$\sigma_{av} = 1.9 \times 10^{-2} [\text{m}/(s^2\sqrt{\text{Hz}})]$ $\sigma_{au} = 1.2 \times 10^{-2} [\text{m}/(s^3\sqrt{\text{Hz}})]$

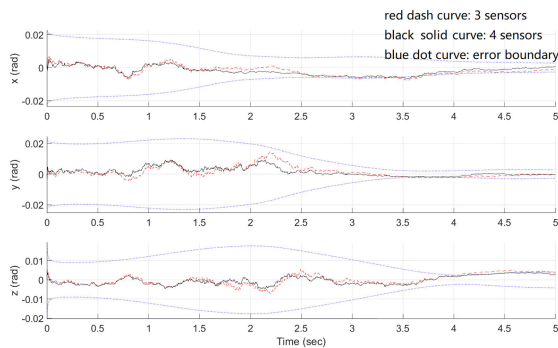


FIGURE 15. The attitude error of the EKF with three sensors.

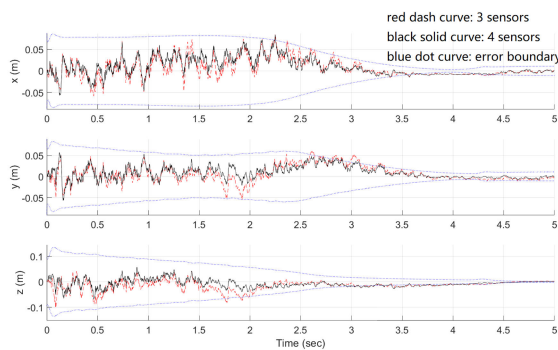


FIGURE 16. The translation error of the EKF with three sensors.

sensors on each body for comparison shown as the black solid curve. The initial velocity and biases of the state are set as zero. Because the propagation in EKF is highly nonlinear, the approximation to the first order of the error may causes the error approach or even slightly penetrate the  $3\sigma$  bound. The precision of the attitude and translation is better than the result of the LM estimator even in the case of three sensors. The errors of attitude and translation are always below 1 deg and 10cm respectively. Besides, adding one more sensor in each body causes only slightly promotion.

C. TRACKING THE END-EFFECTOR OF AN AEROBRIDGE

This subsection simulates the performance of using the modified LS estimator proposed in section V based on the Robotics Toolbox to track a moving aerobridge. To show the practicability, we model the simulation environment as a real airport. Two aerobridges respectively named target and auxiliary are built and shown in Fig. 17. There are two anchors above the roof of the entrances of both aerobridges and one anchor on the top of the terminal building. The topology of the anchor

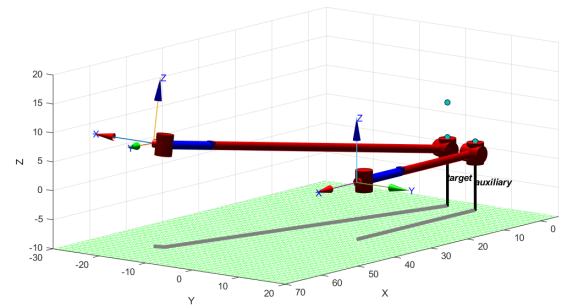


FIGURE 17. Moving aerobridges with attached frame and anchors configuration.

expressed in the reference frame is  $a_1 = [0\ 0\ 1]^T$ ,  $a_2 = [0\ 6\ 1]^T$  and  $a_3 = [0\ 0\ 6]^T$ . Meanwhile, two sensors are on the top of the wrist and the end-effector of the target with 2m separation. We manage to track the trajectory of the end effector of the target w.r.t. the terminal building.

The truth trajectory is given as follows: it rotates  $-15^\circ$  around the shoulder, extends 50m, pitches up  $-7.5^\circ$ , and rotates  $-60^\circ$  around the wrist. All joints of the target move successively. Emulated distances with zero-mean Gaussian-white random noises are generated and the variance is given as  $\sigma = 0.01\text{m}$ . They are sampled with the average interval  $T = 0.02\text{s}$ . The performances of the GN estimator are shown in Fig. 18 and Fig. 19.

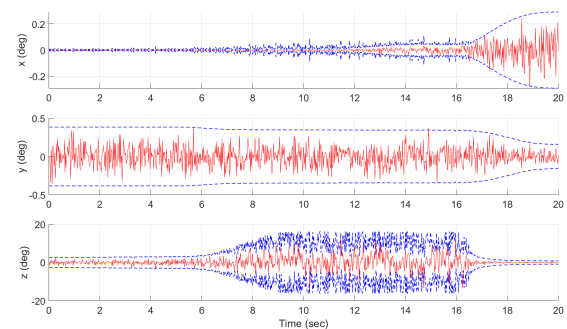


FIGURE 18. The attitude error of GN estimator.

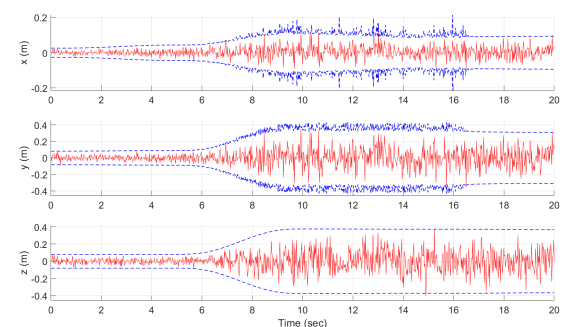


FIGURE 19. The translation error of GN estimator.

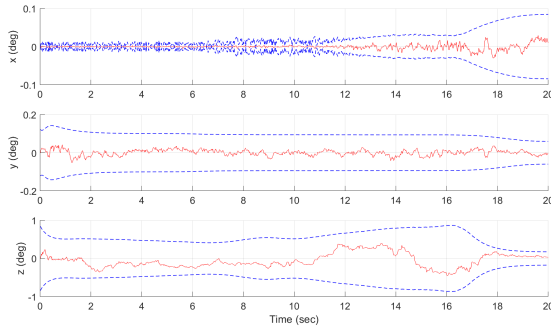


FIGURE 20. The attitude error of MEKF incorporating the pose estimated by the GN estimator.

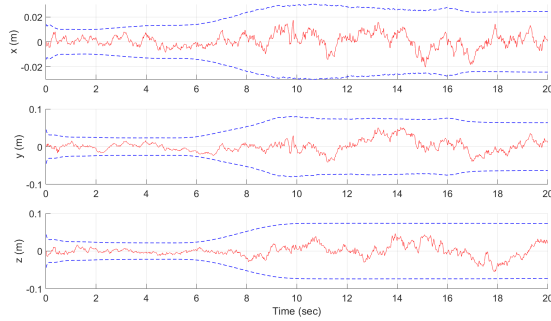


FIGURE 21. The translation error of MEKF incorporating the pose estimated by the GN estimator.

To simulate the real working situation of an aerobridge, we choose a large extension, so the estimation is too noisy to serves as an output. We further use the MEKF [9] to incorporate the angular velocity and linear acceleration measurement form the IMU mounted on the end effector. The parameter of the IMU is shown in table 2 and the performance of the MEKF is illustrated in figure 15. It can reach an accuracy of 1deg for attitude and 0.01m for translation, which is satisfying for practical application.

## VII. CONCLUSION

In this article, based on pairwise range from WSN, we derive a Jacobian matrix of the range measurement w.r.t. the attitude and the translation and further using nonlinear optimization algorithms (GN and LM solver) to iteratively estimate the relative pose. Besides, we propose an unconstrained and lower-dimensional CRLB to numerically verify the performance which outperforms the SVD solution in [14]. To track the relative trajectory of the moving objects, we present a novel relative kinematic without the cumbersome angular acceleration term. It incorporates the IMU and range measurement and outputs a smooth state with associated uncertainty. For objects in three-dimensional space with DOFs less than six, specifically the aerobridge with four DOFs, we provide a simplified algorithm with fewer sensors. We also design three simulations to compare our solver with other existing popular solver, to compare the performance of the

presented GN, LM, and EKF, and to verify the simplified version in the aerobridge setting. The results show the novelty and practicability of our proposed methods.

## APPENDIX A LENGTHY ELEMENTS OF THE $F_k$ AND $G_k$ MATRIX IN EKF

$$F_{21} = -0.5\hat{R}_k^+ \left( \hat{R}_k a_{l,k}^l \right)^\wedge T^2 \quad (80)$$

$$F_{22} = (I_{3 \times 3} + \hat{\omega}_k^+ T) \hat{R}_k^+ \quad (81)$$

$$F_{24} = G_{21} = -\hat{\omega}_k^+ \left( \hat{R}_k^+ \hat{t}_k \right)^\wedge T^2 - \left( \hat{R}_k^+ \hat{t}_k \right)^\wedge T^2 - 0.5 \left[ \hat{R}_k^+ \left( \hat{R}_k a_{l,k}^l - \hat{a}_{f,k}^f \right) \right]^\wedge T^3 \quad (82)$$

$$F_{31} = - (I_{3 \times 3} - 0.5\hat{\omega}_k^+ T) \hat{R}_k^+ \left( \hat{R}_k a_{l,k}^l \right)^\wedge T \quad (83)$$

$$F_{32} = (\hat{\omega}_k^+ - \hat{\omega}_{k+1}^+ - \hat{\omega}_{k+1}^+ \hat{\omega}_k^+ T) \hat{R}_k^+ \quad (84)$$

$$F_{33} = (I_{3 \times 3} - \hat{\omega}_{k+1}^+ T) \hat{R}_k^+ \quad (85)$$

$$F_{35} = G_{33} = (I_{3 \times 3} - 0.5\hat{\omega}_{k+1}^+ T) \hat{R}_k^+ T \quad (86)$$

$$G_{32} = - \left[ (I_{3 \times 3} + \hat{\omega}_k^+ T) \hat{R}_k^+ \hat{t}_k \right]^\wedge - \left( \hat{R}_k^+ \hat{t}_k \right)^\wedge T - 0.5 \left[ \hat{R}_k^+ \left( \hat{R}_k a_{l,k}^l - \hat{a}_{f,k}^f \right) \right]^\wedge T^2 \quad (87)$$

$$F_{34} = (-\hat{\omega}_k^+ + \hat{\omega}_{k+1}^+ \hat{\omega}_k^+ T) \left( \hat{R}_k^+ \hat{t}_k \right)^\wedge T - \left( \hat{\omega}_k^+ \hat{R}_k^+ \hat{t}_k \right)^\wedge T - (2I_{3 \times 3} - \hat{\omega}_{k+1}^+ T) \left( \hat{R}_k^+ \hat{t}_k \right)^\wedge T - (1.5I_{3 \times 3} - 0.5\hat{\omega}_{k+1}^+ T) \left[ \hat{R}_k^+ \left( \hat{R}_k a_{l,k}^l - \hat{a}_{f,k}^f \right) \right]^\wedge T^2 \quad (88)$$

$$G_{31} = (I_{3 \times 3} - \hat{\omega}_k^+ T + \hat{\omega}_{k+1}^+ \hat{\omega}_k^+ T^2) \left( \hat{R}_k^+ \hat{t}_k \right)^\wedge - (I_{3 \times 3} - \hat{\omega}_{k+1}^+ T) \left( \hat{R}_k^+ \hat{t}_k \right)^\wedge T - (I_{3 \times 3} - 0.5\hat{\omega}_{k+1}^+ T) \left[ \hat{R}_k^+ \left( \hat{R}_k a_{l,k}^l - \hat{a}_{f,k}^f \right) \right]^\wedge T^2 \quad (89)$$

## APPENDIX B DERIVATION OF THE JACOBIAN MATRIX IN SECTION V

The coordinate of the anchor  $A_i$  is given as

$$a_{i|oI}^l = \mathbf{a}_i = [x_i \quad y_i \quad z_i]^T \quad (90)$$

where the superscript and subscript are omitted for concision and  $\mathbf{b}_j = \mathbf{b}_{j|oI}^l$  for the mobile nodes  $M_j$ . The distance between  $M_1$  and each anchor is

$$d_{i3} = \|\mathbf{a}_i - \mathbf{b}_3\| = a_1^2 + d_3^2 + \|\mathbf{a}_i\|^2 - a_1 d_3 s_2 + 2a_1 (x_i c_1 + y_i s_1) + 2d_3 (x_i c_1 s_2 + y_i s_1 s_2 + z_i c_2) \quad (91)$$

It is noted that the bold face and light face standard for coordinate vector and DH parameter respectively. The partial derivative of  $d_{i3}$  w.r.t. all joint variables are

$$\frac{\partial d_{i3}}{\partial \theta_1} = \frac{1}{2d_{i3}} [2a_1 (x_i s_1 - y_i c_1) + 2d_3 (-x_i s_1 s_2 + y_i c_1 s_2)] \quad (92)$$



$$\frac{\partial d_{i3}}{\partial \theta_2} = \frac{1}{2d_{i3}} [-2a_1 d_3 c_2 + 2d_3 (x_i c_1 c_2 + y_i s_1 c_2 - z_i s_2)] \quad (93)$$

$$\frac{\partial d_{i3}}{\partial d_3} = \frac{1}{2d_{i3}} [2d_3 - a_1 s_2 + 2(x_i c_1 s_2 + y_i s_1 s_2 + z_i c_2)] \quad (94)$$

$$\frac{\partial d_{i3}}{\partial \theta_4} = 0 \quad (95)$$

The distance between  $M_2$  and each anchor is

$$\begin{aligned} d_{i4} &= \|\mathbf{a}_i - \mathbf{b}_4\| \\ &= a_1^2 + a_4^2 + d_3^2 + \|\mathbf{a}_i\|^2 - 2a_4 d_3 s_4 + 2a_1 a_4 s_2 s_4 \\ &\quad - 2a_4 [x_i (c_1 s_2 s_4 - s_1 c_4) + y_i (s_1 s_2 s_4 + c_1 c_4) + z_i c_2 s_4] \\ &\quad - 2a_1 d_3 s_2 + 2d_3 (x_i c_1 s_2 + y_i s_1 s_2 + z_i c_2) \\ &\quad - 2a_1 (x_i c_1 + y_i s_1) \end{aligned} \quad (96)$$

The partial derivative of  $d_{i4}$  w.r.t. all joint variables are

$$\begin{aligned} \frac{\partial d_{i4}}{\partial \theta_1} &= \frac{1}{2d_{i4}} \{-2a_4 [x_i (-s_1 s_2 s_4 - c_1 c_4) + y_i (c_1 s_2 s_4 - s_1 c_4)] \\ &\quad + 2d_3 (-x_i s_1 s_2 + y_i c_1 s_2) - 2a_1 (-x_i s_1 + y_i c_1)\} \end{aligned} \quad (97)$$

$$\begin{aligned} \frac{\partial d_{i4}}{\partial \theta_2} &= \frac{1}{2d_{i4}} [2a_1 a_4 c_2 s_4 - 2a_4 (x_i c_1 c_2 s_4 + y_i s_1 c_2 s_4 - z_i s_2 s_4) \\ &\quad - 2a_1 d_3 c_2 + 2d_3 (x_i c_1 c_2 + y_i s_1 c_2 - z_i s_2)] \end{aligned} \quad (98)$$

$$\begin{aligned} \frac{\partial d_{i4}}{\partial d_3} &= \frac{1}{2d_{i4}} [2d_3 - 2a_4 s_4 - 2a_1 s_2 \\ &\quad + 2(x_i c_1 s_2 + y_i s_1 s_2 + z_i c_2)] \end{aligned} \quad (99)$$

$$\begin{aligned} \frac{\partial d_{i4}}{\partial \theta_4} &= \frac{1}{2d_{i4}} \{(-2a_4 d_3 + 2a_1 a_4 s_2) c_4 \\ &\quad - 2a_4 [x_i (c_1 s_2 c_4 + s_1 s_4) + y_i (s_1 s_2 c_4 - c_1 s_4) \\ &\quad + z_i c_2 c_4]\} \end{aligned} \quad (100)$$

## REFERENCES

- [1] S. Chen and K. C. Ho, "Accurate localization of a rigid body using multiple sensors and landmarks," *IEEE Trans. Signal Process.*, vol. 63, no. 24, pp. 6459–6472, Dec. 2015.
- [2] S. Chen and K. C. Ho, "Localization of a mobile rigid sensor network," in *Proc. 24th Eur. Signal Process. Conf. (EUSIPCO)*, Budapest, Hungary, Aug. 2016, pp. 1368–1372.
- [3] S. P. Chepuri, G. Leus, and A.-J. van der Veen, "Position and orientation estimation of a rigid body: Rigid body localization," in *Proc. IEEE Int. Conf. Acoust., Speech Signal Process.*, May 2013, pp. 5185–5189.
- [4] S. P. Chepuri, A. Simonetto, G. Leus, and A.-J. van der Veen, "Tracking position and orientation of a mobile rigid body," in *Proc. 5th IEEE Int. Workshop Comput. Adv. Multi-Sensor Adapt. Process. (CAMSAP)*, Dec. 2013, pp. 37–40.
- [5] G. Wahba, "A least squares estimate of satellite attitude," *SIAM Rev.*, vol. 7, no. 3, p. 409, Jul. 1965.
- [6] B. K. P. Horn, "Closed-form solution of absolute orientation using unit quaternions," *J. Opt. Soc. Amer. A, Opt. Image Sci.*, vol. 4, no. 4, pp. 629–642, 1987.
- [7] H. D. Black, "A passive system for determining the attitude of a satellite," *AIAA J.*, vol. 2, no. 7, pp. 1350–1351, Jul. 1964.
- [8] J. E. Keat, "Analysis of least-squares attitude determination routine DOAOP," *Comput. Sci. Corp.*, Tysons, VI, USA, Tech. Rep. CSC/TM-77/6034, Feb. 1977.
- [9] H.-L. Pei and R. Xia, "Ranging-aided relative navigation of multi-platforms," *Control Theory Technol.*, vol. 16, no. 2, pp. 122–132, May 2018.
- [10] F. L. Markley and J. L. Crassidis, *Fundamentals of Spacecraft Attitude Determination and Control*. New York, NY, USA: Springer, 2014.

- [11] J. L. Crassidis and J. L. Junkins, *Optimal Estimation of Dynamic Systems*, 2nd ed. London, U.K.: Chapman & Hall, 2004.
- [12] S.-G. Kim, J. L. Crassidis, Y. Cheng, A. M. Fosbury, and J. L. Junkins, "Kalman filtering for relative spacecraft attitude and position estimation," *J. Guid., Control, Dyn.*, vol. 30, no. 1, pp. 133–143, Jan. 2007.
- [13] A. M. Fosbury and J. L. Crassidis, "Relative navigation of air vehicles," *J. Guid., Control, Dyn.*, vol. 31, no. 4, pp. 824–834, Jul. 2008.
- [14] S. P. Chepuri, G. Leus, and A.-J. van der Veen, "Rigid body localization using sensor networks," *IEEE Trans. Signal Process.*, vol. 62, no. 18, pp. 4911–4924, Sep. 2014.
- [15] J. Jiang, G. Wang, and K. C. Ho, "Accurate rigid body localization via semidefinite relaxation using range measurements," *IEEE Signal Process. Lett.*, vol. 25, no. 3, pp. 378–382, Mar. 2018.
- [16] J. Jiang, G. Wang, and K. C. Ho, "Sensor network-based rigid body localization via semi-definite relaxation using arrival time and Doppler measurements," *IEEE Trans. Wireless Commun.*, vol. 18, no. 2, pp. 1011–1025, Feb. 2019.
- [17] G. S. Chirikjian, *Stochastic Models, Information Theory, and Lie Groups: Analytic Methods and Modern Applications*, vol. 2. Cham, Switzerland: Springer, 2011.
- [18] L. Kavan, S. Collins, C. O'Sullivan, and J. Zara, "Dual quaternions for rigid transformation blending," Trinity College Dublin, Dublin, Ireland, Tech. Rep. TCD-CS-2006-46, 2006.
- [19] J. M. Lee, "Smooth manifolds," in *Introduction to Smooth Manifolds* (Graduate Texts in Mathematics), vol. 218. New York, NY, USA: Springer, 2013, doi: 10.1007/978-1-4419-9982-5\_1.
- [20] T. D. Barfoot, *State Estimation for Robotics*. Cambridge, U.K.: Cambridge Univ. Press, 2017.
- [21] K. Madsen, H. B. Nielsen, and O. Tingleff, *Methods for Non-Linear Least Squares Problems*. Lyngby, Denmark: Technical Univ. of Denmark, Informatics and Mathematical Modelling, 2004. [Online]. Available: <http://www2.imm.dtu.dk/pubdb/pubs/3215-full.html>
- [22] S. M. Kay, *Fundamentals of Statistical Signal Processing*. Upper Saddle River, NJ, USA: Prentice-Hall, 1993.
- [23] J. Nocedal and S. Wright, *Numerical Optimization*. Cham, Switzerland: Springer, 2006.
- [24] *P440 UWB Module*. Accessed: Jun. 2017. [Online]. Available: <http://www.timedomain.com>
- [25] *Multilateration*. Accessed: Mar. 2018. [Online]. Available: <https://en.wikipedia.org/wiki/Multilateration>



**RUICAN XIA** was born in China, in 1993. He received the bachelor's degree (Hons.) in electrical engineering and automation from the Dongguan University of Technology, Dongguan, China, in 2016. He is currently pursuing the Ph.D. degree with the Key Laboratory of Autonomous Systems and Network Control, Ministry of Education, South China University of Technology. Since September 2016, he has been with the Key Laboratory of Autonomous Systems and Network Control, Ministry of Education, South China University of Technology. His research interests include relative navigation of satellites and indoor positioning.



**HAILONG PEI** (Member, IEEE) received the bachelor's and master's degrees from Northwestern Polytechnical University, China, in 1986 and 1989, respectively, and the Ph.D. degree from the South China University of Technology, China, in 1992. He is currently a Professor with the School of Automation Science and Engineering, South China University of Technology, and the Director of the Key Laboratory of Autonomous Systems and Network Control, Ministry of Education, and the Unmanned System Engineering Center of Guangdong Province. He works on unmanned aerial systems and robotic control. He serves as the Deputy Editor-in-Chief for the *Journal of Control Theory and Applications* and an Associate Editor for *Journal of Intelligent and Robotic Systems and Acta Automatica Sinica*.

...